Machine learning for atherosclerotic tissue component classification in combined near-infrared spectroscopy intravascular ultrasound imaging: Validation against histology

Bajaj, R.; Eggermont, J.; Grainger, S.J.; Raber, L.; Parasa, R.; Khan, A.H.A.; ... ; Bourantas, C.V.

Atherosclerosis 345 (2022) 15–25

Contents lists available at ScienceDirect

Atherosclerosis

journal homepage: www.elsevier.com/locate/atherosclerosis

Machine learning for atherosclerotic tissue component classification in combined near-infrared spectroscopy intravascular ultrasound imaging: Validation against histology

Retesh Bajaj [a,b], Jeroen Eggermont [c], Stephanie J. Grainger [d], Lorenz Räber [e], Ramya Parasa [a,b], Ameer Hamid A. Khan [a], Christos Costa [a], Emrah Erdogan [a], Michael J. Hendricks [d], Karthik H. Chandrasekharan [a,b], Mervyn Andiapen [a,b], Patrick W. Serruys [f], Ryo Torii [g], Anthony Mathur [a,b], Andreas Baumbach [a,b], Jouke Dijkstra [c], Christos V. Bourantas [a,b,h,*]

[a] Department of Cardiology, Barts Heart Centre, Barts Health NHS Trust, London, UK
[b] Cardiovascular Devices Hub, Centre for Cardiovascular Medicine and Devices, William Harvey Research Institute, Queen Mary University of London, UK
[c] Division of Imaging Processing, Department of Radiology, Leiden University Medical Center, Leiden, the Netherlands
[d] Infraredx, Inc., Bedford, MA, USA
[e] Department of Cardiology, Bern University Hospital, Bern, Switzerland
[f] Faculty of Medicine, National Heart & Lung Institute, Imperial College London, UK
[g] Department of Mechanical Engineering, University College London, London, UK
[h] Institute of Cardiovascular Sciences, University College London, London, UK

ARTICLE INFO

Keywords:
Intravascular ultrasound
Near-infrared spectroscopy
Plaque characterization
Machine learning

ABSTRACT

Background and aims: Accurate classification of plaque composition is essential for treatment planning. Intravascular ultrasound (IVUS) has limited efficacy in assessing tissue types, while near-infrared spectroscopy (NIRS) provides complementary information to IVUS but lacks depth information. The aim of this study is to train and assess the efficacy of a machine learning classifier for plaque component classification that relies on IVUS echogenicity and NIRS-signal, using histology as reference standard.

Methods: Matched NIRS-IVUS and histology images from 15 cadaveric human coronary arteries were analyzed (10 vessels were used for training and 5 for testing). Fibrous/pathological intimal thickening (F-PIT), early necrotic core (ENC), late necrotic core (LNC), and calcific tissue regions-of-interest were detected on histology and superimposed onto IVUS frames. The pixel intensities of these tissue types from the training set were used to train a J48 classifier for plaque characterization (ECHO-classification). To aid differentiation of F-PIT from necrotic cores, the NIRS-signal was used to classify non-calcific pixels outside yellow-spot regions as F-PIT (ECHO-NIRS classification). The performance of ECHO and ECHO-NIRS classifications were validated against histology.

Results: 262 matched frames were included in the analysis (162 constituted the training set and 100 the test set). The pixel intensities of F-PIT and ENC were similar and thus these two tissues could not be differentiated by echogenicity. With ENC and LNC as a single class, ECHO-classification showed good agreement with histology for detecting calcific and F-PIT tissues but had poor efficacy for necrotic cores (recall 0.59 and precision 0.29). Similar results were found when F-PIT and ENC were treated as a single class (recall and precision for LNC 0.78 and 0.33, respectively). ECHO-NIRS classification improved necrotic core and LNC detection, resulting in an increase of the overall accuracy of both models, from 81.4% to 91.8%, and from 87.9% to 94.7%, respectively. Comparable performance of the two models was seen in the test set where the overall accuracy of ECHO-NIRS classification was 95.0% and 95.5%, respectively.

Conclusions: The combination of echogenicity with NIRS-signal appears capable of overcoming limitations of echogenicity, enabling more accurate characterization of plaque components.

* Corresponding author. Barts Heart Centre, West Smithfield, London, EC1A 7BE, UK.
E-mail address: cbourantas@gmail.com (C.V. Bourantas).

https://doi.org/10.1016/j.atherosclerosis.2022.01.021
Received 23 September 2021; Received in revised form 9 January 2022; Accepted 27 January 2022
Available online 29 January 2022

1. Introduction

The assessment of coronary plaque composition is essential in treatment planning and predicting cardiovascular events. Calcific atherosclerotic plaques have been associated with a higher risk of procedural complications, stent underexpansion and suboptimal percutaneous coronary intervention (PCI) results [1], [[,2] while lipid-rich lesions appear to be associated with non-reflow and peri-procedural myocardial infarction [3–5]. Furthermore, cumulative data have demonstrated that lipid-rich atherosclerotic plaques are vulnerable lesions and predict future adverse cardiovascular events [6–9].

Over recent years several methodologies aiming to accurately characterize and quantify plaque components in intravascular imaging have been introduced. Echogenicity [10] and radiofrequency backscatter analysis [11–13] were the first approaches proposed for reliable detection of different tissue types in intravascular ultrasound (IVUS) while in optical coherence tomography (OCT), backscatter and attenuation coefficient analysis [14–16] of the reflected signal, as well as machine learning techniques [17,18] have been proposed. However, none of them have found broad application in current clinical practice due to a lack of widely available, user-friendly software incorporating these methodologies or robust and consistent histological evidence to support their accuracy.

To address this unmet need, near-infrared spectroscopy (NIRS)-IVUS has been introduced. NIRS-IVUS appears capable of overcoming the limitations of standalone intravascular imaging as NIRS can accurately identify necrotic core (NC) tissue, while IVUS can detect the presence of calcium [19]. However, while NIRS can estimate the circumferential arc of NC, it is unable to provide explicit depth information, differentiate superficial from deeply-embedded NC tissue and assess its area and volumetric burden. Similarly, there is no methodology today for the automated quantification of the calcific tissue in IVUS images.

The aim of this study is to investigate for the first time the efficacy of tissue echogenicity combined with NIRS in accurately detecting distribution of plaque components and quantifying their burden, using histology as reference standard.

2. Materials and methods

2.1. Studied patients

We retrospectively analyzed NIRS-IVUS and histological data from excised cadaver hearts collected in a previously described study that aimed to examine the efficacy of NIRS imaging in detecting NC [International Institute for the Advancement of Medicine, Edison, NJ, and Asterand Bioscience (BioIVT), Detroit, MI] [20]. Donated hearts were received within 48 h of death, with intravascular imaging performed within 96 h. Totally occluded segments and those with minimum luminal diameter <1 mm were excluded as the NIRS-IVUS catheter could not be advanced in these segments. The remaining segments were mounted on a fixture and perfused with human blood at body temperature, with pulsatile flow by means of a pump at 60 cycles/minute (coronary pressure 80–120 mmHg). NIRS-IVUS imaging was performed using the 3.2-F 40 MHz TVC Imaging System NIRS-IVUS catheter (Infraredx, Bedford, Massachusetts) which was advanced to the distal part of the vessel over a 0.014-inch guidewire and then was pulled back at a fixed speed of 0.5 mm/s. Following intravascular imaging, studied vessels were pressure-fixed in formalin, and segmented at 2-mm intervals; two 7 μm histopathology slides were taken at every interval and were stained with hematoxylin-eosin and Russell-Movat's pentachrome [Mass Histology Service (now Horus Scientific), Worcester, MA], respectively. From this data, 15 coronary arteries with increased lipid-rich segments (presence of yellow signal in ≥ 1 quadrant for a length of at least 16 mm in NIRS-IVUS) were selected and included in the analysis.

2.2. Histological analysis

The matching between histological and NIRS-IVUS cross-sections was performed by two experts (RB & CVB) (Supplementary Fig. 1). The distance of the IVUS and histological sections from the distal end of the studied segment, anatomical landmarks (i.e., presence of side-branches and calcification) and plaque eccentricity were used to identify correspondence between NIRS-IVUS and histology. Sectioning or imaging artefacts that made visualization of the entire plaque impossible and IVUS images with insufficient quality were excluded from the analysis.

The matched histological images were analyzed by an experienced histopathologist blinded to the intravascular imaging data. Within each slide, the following tissue types were identified: pathological intimal thickening (PIT) characterized by smooth muscle cells in a proteoglycan-rich matrix with extracellular lipid pools without necrosis, fibrotic tissue (FT) consisting of smooth muscle cells, collagen fibers and proteoglycans, early necrotic core (ENC) defined as an acellular extracellular lipid pool with early necrosis and few cholesterol clefts, late necrotic core (LNC) consisting of an acellular lipid core with advanced necrosis and extensive cholesterol clefts, and calcific tissue [21,22]. Regions with these tissue types were annotated, with PIT and fibrous tissue (F-PIT) merged in one class; in cases where calcific tissue overlapped with ENC or LNC the region was classified as calcific.

2.3. IVUS analysis

Segmentation of the IVUS frames matched with histological cross-sections was performed by an expert analyst using the QCU-CMS software (Version 4.69, Leiden University Medical Center, Leiden, the Netherlands) in accordance with established guidelines, annotating the external elastic membrane (EEM) and lumen borders and defining the plaque area [23].

2.4. Co-registration of the NIRS-IVUS and histological cross-sections

The histological cross-sections were superimposed onto the corresponding IVUS images and the identified tissue types were used to delineate four regions of interest (ROI): F-PIT, ENC, LNC and calcific tissue. Each ROI corresponded to a single tissue type; in cases where calcification overlapped with ENC or LNC the ROI was classified as calcific since in these mixed plaques, tissue behavior is predominantly affected by the presence of calcium. F-PIT, ENC, LNC and calcific ROIs did not overlap. In areas with lack of IVUS signal (i.e., behind calcific tissue or in cases of a guide-wire artifact), no ROIs were annotated. From this dataset, the NIRS-IVUS and histological cross sections acquired from 10 coronary arteries (from 9 hearts) were used to develop and train a machine learning classifier for plaque component classification (training set), and the remaining 5 vessels (from 4 hearts) to test the performance of the trained classifier (test set).

2.5. Machine learning classifier training for echogenicity-based tissue classification

In the training set a previously described methodology for automated echogenicity analysis that relies on the identification of pixel intensity cut-offs in relation to the adventitia intensity was used to define plaque composition [24]. This approach calculates the vessel adventitia pixel intensities and their median value is used for discriminating tissue types assuming that the grey-pixel intensity of ENC and LNC tissue is lower than that of the adventitia, the intensity of F-PIT tissue is similar or higher to adventitia and that the calcific tissue has a higher pixel intensity than the adventitia and is accompanied by acoustic shadowing behind.

To further optimize the performance of the echogenicity approach, we modified the original methodology and used in the training set the ROIs defined in the co-registered NIRS-IVUS images with the

histological cross-sections to estimate the best pixel intensity cut-offs of the 4 different tissue types. The mean, standard deviation, median, skewness, and kurtosis values of the grey-pixel intensity in each region were extracted and used to train a machine learning classifier algorithm.

The absolute mean tissue intensity in each ROI was used for tissue classification as this resulted in the best model performance of the various attributes tested (results not shown). Based on training data, a J48 classifier model was selected as its performance was superior in comparison to other models (Supplementary Table 1). To improve the detection of the calcific tissue, a shadow detection algorithm behind pixels with a high intensity was incorporated.

Three different tissue classification models were built: the 1st included the four tissue types as distinct classes, in the 2nd model, ENC and LNC were merged into a single class – the NC class, while the 3rd model focused on the differentiation of the LNC, which is regarded as the most advanced high-risk tissue type, from the F-PIT and ENC, which were merged into a single class. For each of the 3 models, the best pixel intensity cut-off for the defined classes were identified based on 10-fold cross-validation and used for optimization of a decision tree for tissue classification (Supplementary Fig. 2).

Two methodologies were used to characterize plaque composition. In the first, the echogenicity (ECHO)-based approach, tissue classification was performed based on pixel intensity. In the second methodology, the echogenicity and NIRS (ECHO-NIRS) approach, the IVUS and the NIRS information were combined for more accurate plaque characterization. More specifically, a post-processing step was added to the echogenicity analysis: the NIRS-signal was used to identify areas with high probability of necrotic core tissue (yellow-spots) and in these, tissue characterization was performed using pixel intensity while in non-yellow-spot areas, non-calcific tissue classifications were considered to be F-PIT.

Classification algorithms were trained and validated on Weka software version 3.8 (University of Waikato, New Zealand).

2.6. Comparison of histology and NIRS-IVUS estimations

Two types of comparison were made between the estimations of NIRS-IVUS and histology, which was treated as the reference standard:

- Region-level analysis: in this analysis, the pixels enclosed in the defined ROI were classified according to their intensity – in the ECHO-NIRS approach, the yellow-spot distribution was also considered for pixel classification. The predominant estimated tissue type in each ROI was used for classification of the entire region.
- Area-level analysis: in this analysis the % of each estimated tissue type was calculated in the ROIs and the % of the correct estimations according to the histological classification was reported.

2.7. Statistical methods

Continuous variables are reported as mean ± SD and categorical variables as absolute numbers and percentages. The Kolmogorov-Smirnov test was used to examine the distribution of continuous variables; normally distributed variables were compared using student's *t*-test, while the Mann-Whitney *U* test was used for two set comparison in the non-normally distributed variables.

The performance of the classifier was examined by calculating the recall, precision and F-score for each class. The recall or sensitivity is calculated as: true positive/(true positive + false negative), the precision as: true positive/(true positive + false positive), and the F-score which is the harmonic mean of recall and precision is calculated as 2 x [sensitivity x precision/(sensitivity + precision)], with a maximum score of 1.0 indicating perfect precision and recall [25,26].

The overall classifier performance was reported as the weighted average of recall, precision and F-score. The weighted average is a common method for reporting the efficacy of a methodology in multi-classifier tasks and takes into account the performance of the classifier for each class and the relative proportion of each class in the dataset to estimate the overall performance of the classifier. The accuracy of the classifier was calculated as the percentage of correct classifications of all classifications made by the model. A p-value of <0.05 was taken to be statistically significant. Statistical analyses were performed using SPSS for Mac version 23 (IBM, Armonk, New York) and MedCalc software version 19.1.6 (Ostend, Belgium).

3. Results

Fifteen coronary arteries from thirteen autopsied hearts were included in the analysis. Baseline heart donor demographics are shown in Supplementary Table 2 and baseline IVUS measurements in Supplementary Table 3. The mean lengths of the studied segments was 46.0 ± 12.5 mm for the training set and 51.3 ± 8.4 mm for the test set, providing 346 histological sections for matching (220 for the training set and 126 for the test set). From these, 42 histological sections were excluded because of sectioning artefacts, 26 sections were excluded because of the presence of artefacts in the corresponding IVUS images preventing reliable analysis, and 16 due to inability to reliably match these with a corresponding IVUS frame. Therefore, 162 histological cross-sections in the training set and 100 in the test set were successfully matched with NIRS-IVUS frames and included in the final analysis. In the training set images, 349 ROIs were annotated: 207 F-PIT, 31 ENC, 49 LNC and 62 calcific. ENC and LNC were seen predominately in yellow-spot regions compared to F-PIT and calcific tissue (Supplementary Table 4). In the test set, 201 ROIs were annotated including 111 F-PIT, 27 ENC, 19 LNC and 44 calcific.

3.1. Pixel intensity of the four tissue types in the training set

The pixel intensity data of the 4 tissue types are shown in Supplementary Table 4 and Fig. 1. ROIs classified as calcific had the highest pixel intensity following by F-PIT, ENC and LNC. Comparison of the mean pixel intensities of the ROIs showed statistically significant differences for all tissue types; however, there was an overlap in the pixel intensities of ENC and F-PIT ROIs (Fig. 1).

3.2. Tissue classification based on the information provided by echogenicity in the training set

None of the tested classifiers were able to distinguish ENC from F-PIT tissue, due to the overlap of the pixel intensities of these two tissue types; therefore, differentiation of the 4 tissue types was not possible with echogenicity (Fig. 1 and Supplementary Table 1).

When ENC and LNC were treated as a single class (NC), the model in region-level analysis had, overall, an excellent recall, precision, F-score and accuracy in correctly characterizing ROIs. However, the performance of the model for the identification of the NC was weak as it misclassified half of these ROIs as F-PIT. Conversely, the model had excellent efficacy in detecting F-PIT and calcific ROIs (Table 1). Results were similar in area-level analysis. ECHO-classification had an overall accuracy of 81.4% in detecting different tissue types; however, the model had poor efficacy in detecting NC tissue which was often misclassified as F-PIT, and moderate efficacy in classifying calcific ROI pixels, 23% of which were misclassified as F-PIT (Table 1).

Notably, the performance of the echogenicity approach based on previously described thresholds of pixel intensity relative to median adventitia pixel intensity for detecting F-PIT, NC (i.e., ENC and LNC) and calcific tissue was inferior to the above results with the overall accuracy at region- and area-level analysis estimated only 47.9% and 41.9%, respectively (Supplementary Table 5).

When F-PIT and ENC were treated as a single class, the classifier in region-level analysis had an excellent overall accuracy of 93.7% in characterizing ROIs. The model was able to detect F-PIT/ENC and

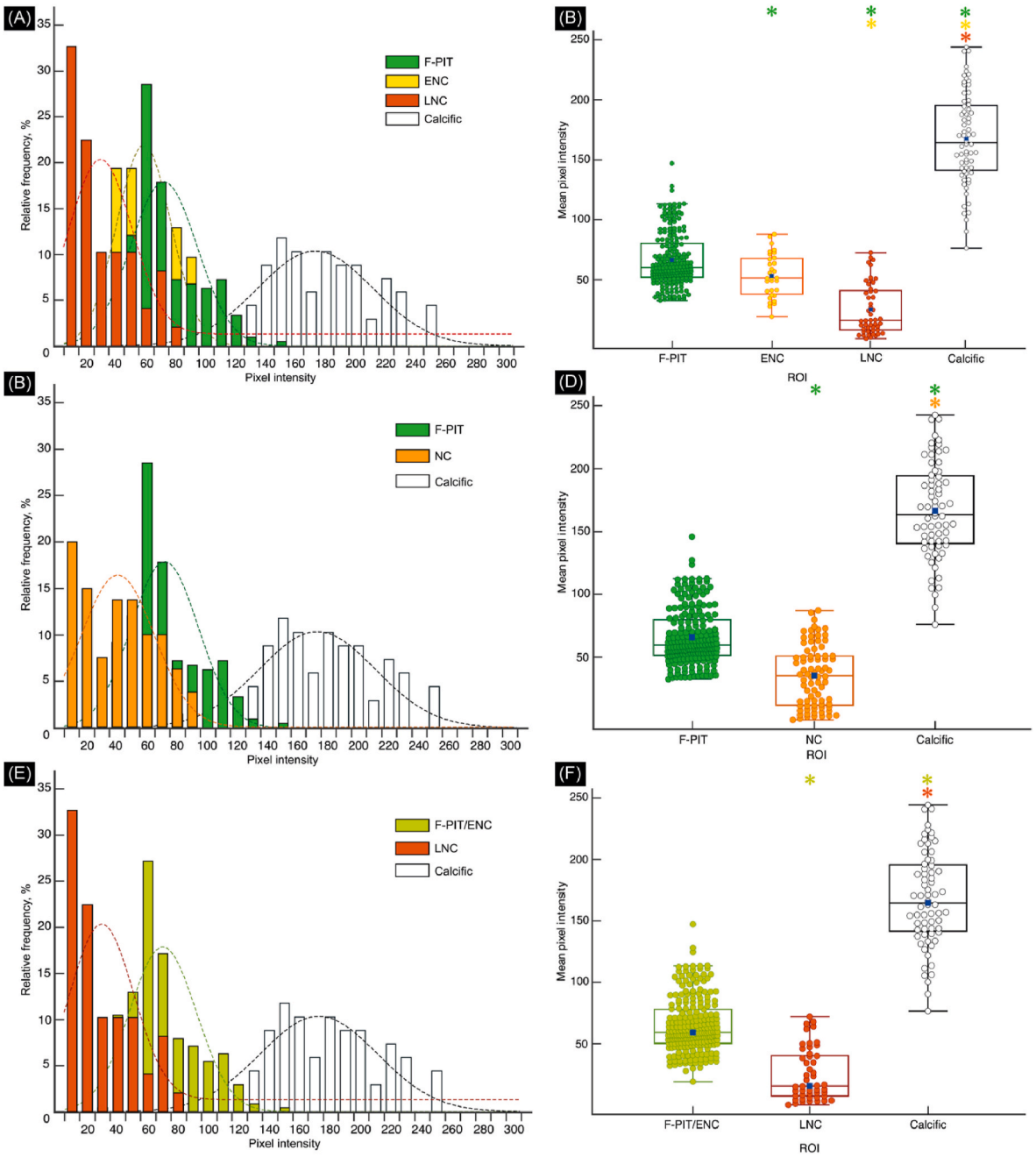

Fig. 1. Mean pixel intensities of the ROIs of the different tissue types.
(A) Histogram with the relative frequency of the mean pixel intensities of the ROIs for the 4 tissue types; a normal distribution line has been fitted for each tissue class representing its average pixel intensity as the peak (A). (B) A box-and-whisker plot representing the median, interquartile ranges and overall range of the mean pixel intensity of the ROIs for the 4 tissue types with the blue dots representing the mean pixel intensities; * indicates statistically significant ($p < 0.05$) difference in the mean pixel intensity between tissue types; green * indicates significant difference when compared to F-PIT, yellow * indicates significant difference when compared to ENC and red * indicates significant difference compared to LNC. (C) The mean pixel intensities, with normal distribution lines, of the ROIs when the ENC and LNC were merged in a single class (NC), and (D) the corresponding box-and-whisker plots for the 3 classes with * indicating significant difference between tissue classes; green * indicates significant difference when compared to F-PIT, and orange * when compared to NC. (E) The mean pixel intensities, with normal distribution lines, of the ROIs when the F-PIT and ENC were merged in a single class, and (F) the corresponding box-and-whisker plots for the 3 classes with * indicating significant difference between tissue classes; light green * indicates significant difference when compared to F-PIT/ENC, and red * indicates significant difference compared to LNC. (For interpretation of the references to colour in this figure legend, the reader is referred to the Web version of this article.)

calcific ROIs with recall, precision and F-score ≥0.93, while for LNC the model misclassified 1/3 of the cases as F-PIT/ENC.

In area-level analysis, the classification performance of the model was again high with an overall accuracy of 87.9%. F-PIT/ENC tissue detection was very accurate; however, for LNC tissue the model had low precision and F-score; in addition, the efficacy of the model for classifying calcific tissue was as before, moderate (Table 2).

3.3. *Tissue classification based on the combined information provided by echogenicity and NIRS in the training set*

The information provided by NIRS with regards to the presence of NC

Table 1
Confusion matrix and classifier performance in region- and area-level analysis with 3 tissue types (ENC and LNC were combined in the NC class) based on ECHO and ECHO-NIRS classification in the training set.

		Histological classification			Validation metrics			
		F-PIT	NC	Calcific	Recall	Precision	F-score	Accuracy (%)
ECHO-classification	**Region-level analysis**							
	F-PIT	199	40	2	0.96	0.83	0.89	-
	NC	7	39	0	0.49	0.85	0.62	-
	Calcific	1	1	60	0.97	0.97	0.97	-
	Overall performance	-	-	-	0.85	0.86	0.84	85.4
	Area-level analysis							
	F-PIT (mm^2)	527.79	25.14	4.75	0.84	0.95	0.89	-
	NC (mm^2)	91.99	37.77	0.08	0.59	0.29	0.39	-
	Calcific (mm^2)	9.29	1.45	15.45	0.76	0.59	0.66	-
	Overall performance	-	-	-	0.81	0.88	0.84	81.4
ECHO-NIRS classification	**Region-level analysis**							
	F-PIT	203	44	2	0.98	0.82	0.89	-
	NC	3	34	0	0.43	0.92	0.58	-
	Calcific	1	2	60	0.97	0.95	0.96	-
	Overall performance	-	-	-	0.85	0.86	0.83	85.1
	Area-level analysis							
	F-PIT (mm^2)	608.18	31.34	4.79	0.97	0.94	0.96	-
	NC (mm^2)	11.60	31.57	0.04	0.49	0.73	0.59	-
	Calcific (mm^2)	9.29	1.45	15.45	0.76	0.59	0.66	-
	Overall performance	-	-	-	0.92	0.91	0.91	91.8

F-PIT, fibrotic or pathological intimal thickening; NC, necrotic core.

tissue did not appear to affect the overall performance of the model that was built to differentiate F-PIT, NC and calcific ROIs (Table 1). However, in area-level analysis the precision and the F-score for F-PIT and NC detection improved while results were similar for calcific tissue detection. The performance of the ECHO-NIRS classifier in area-level analysis was superior to ECHO-classification with recall, precision and F-score of 0.92, 0.91 and 0.91, respectively, and an overall accuracy of 91.8%.

Similar findings were noted for model performance when F-PIT and ENC were merged in a single class (Table 2). The overall performance of the classifier for accurately detecting ROIs was high – similar to the performance of the ECHO-model – despite the fact that the LNC was misclassified as F-PIT/ENC in 37% of the cases. In area-level analysis, ECHO-NIRS classification resulted in more accurate detection of F-PIT/ENC and LNC tissue than ECHO-classification, resulting in a significant improvement of the accuracy of the model from 87.9% to 94.7%.

Tissue classification with both the ECHO and ECHO-NIRS methodologies was found to be rapid, with an average 2000-frame IVUS pullback segmented every 0.5 mm (65 frames) analyzed within 5 s (on a desktop PC with an Intel Core i5 processor and 8 GB of RAM).

3.4. Tissue classification performance in the independent test set

The performance of the trained classifiers was examined in the test set consisting of 201 ROIs in 100 NIRS-IVUS frames matched with histological cross-sections. ECHO-classification using the classifier trained for NC detection showed a similar performance to the training set with overall accuracy in region-level analysis of 82.6% and in area-level analysis of 71.6%. ECHO-NIRS classification improved accuracies to 88.6% and 95.0%, respectively. In the test set, ECHO-NIRS classification had a higher recall, precision and F-score for region-level NC detection compared to the training set. The performance of ECHO-NIRS classification was similar in training and test sets for F-PIT and calcific tissue detection in region-level analysis, while in area-level analysis ECHO-NIRS classification enabled more accurate estimation of calcific area in the test set (Table 3).

In the model trained for LNC detection, the overall performance of ECHO and ECHO-NIRS classification was comparable to the training set with overall region-level accuracies of 84.6% and 91.5% and area-level accuracies of 75.1% and 95.5%, respectively. In this set, 6% of F-PIT/ENC ROIs were misclassified as LNC; this had an impact in the precision

Table 2
Confusion matrix and classifier performance in region and area-level analysis with 3 tissue types (F-PIT and ENC were combined in a single class) based on ECHO-classification and ECHO-NIRS classification in the training set.

		Histological classification			Validation metrics			
		F-PIT/ENC	LNC	Calcific	Recall	Precision	F-score	Accuracy (%)
ECHO-classification	**Region-level analysis**							
	F-PIT/ENC	235	16	2	0.99	0.93	0.96	-
	LNC	2	32	0	0.65	0.94	0.77	-
	Calcific	1	1	60	0.97	0.97	0.97	-
	Overall performance	-	-	-	0.94	0.94	0.93	93.7
	Area-level analysis							
	F-PIT/ENC (mm^2)	580.25	8.24	4.74	0.89	0.98	0.93	-
	LNC (mm^2)	62.91	31.24	0.05	0.78	0.33	0.47	-
	Calcific (mm^2)	10.27	0.42	15.49	0.76	0.59	0.67	-
	Overall performance	-	-	-	0.88	0.93	0.90	87.9
ECHO-NIRS classification	**Region-level analysis**							
	F-PIT/ENC	236	18	2	0.99	0.92	0.96	-
	LNC	1	30	0	0.61	0.97	0.75	-
	Calcific	1	1	60	0.97	0.97	0.97	-
	Overall performance	-	-	-	0.93	0.94	0.93	93.4
	Area-level analysis							
	F-PIT/ENC (mm^2)	632.94	12.45	4.76	0.97	0.97	0.97	-
	LNC (mm^2)	10.22	27.03	0.03	0.68	0.73	0.70	-
	Calcific (mm^2)	10.27	0.42	15.49	0.76	0.59	0.67	-
	Overall performance	-	-	-	0.95	0.95	0.95	94.7

ENC, early necrotic core; F-PIT, fibrotic or pathological intimal thickening; LNC, late necrotic core.

and F-score of ECHO-NIRS classification for LNC region- and area-level classification, which were reduced compared to the training set. Conversely, ECHO-NIRS classification was similar in training and test sets for F-PIT/ENC and calcific tissue detection in region-level analysis, while in area-level analysis ECHO-NIRS enabled more accurate estimation of calcific area in the test set (Table 4).

4. Discussion

In this study, we examined for the first time the efficacy of echogenicity combined with the information gleaned from NIRS in characterizing plaque composition in NIRS-IVUS images. We found that: 1) NIRS is very sensitive in detecting ENC and LNC tissue, 2) IVUS pixel intensity enables accurate detection of calcific ROIs but it is unable to differentiate F-PIT from ENC and has limited efficacy in detecting LNC ROIs, and 3) the information provided by NIRS improves the efficacy of echogenicity in differentiating F-PIT from NC tissues.

From the early days of IVUS imaging it has been apparent that greyscale pixel intensity provides information about plaque composition. Several histology-based studies have shown that in IVUS images the calcific tissue has increased signal intensity and is associated with acoustic shadowing, the fibrotic tissue has signal intensity that is similar to adventitia, while lipid tissue is often characterized by an echolucent area within the plaque [27–29]. More recent reports have shown that the presence of attenuated plaques is associated with large lipid pools or the presence of NC and is a predictor of adverse events [30–34]. To expedite the quantification of pixel intensity and stratify cardiovascular risk, automated solutions have been developed to classify atherosclerotic lesions as hyper or hypoechogenic using the adventitia as the reference standard [10]. Studies assessing the efficacy of these tools in assessing plaque composition demonstrated conflicting results. In the study of Bruining et al. that included 8 left anterior descending coronary arteries obtained from autopsied hearts, there was no difference in the pixel intensity of different tissue types. However, a more recent analysis performed in 60 lesions obtained from porcine models showed that greyscale pixel intensity classification was superior to virtual histology-IVUS in detecting NC with a sensitivity of 89.7% compared to 41.1%, respectively [35].

The present report is the first that investigates at scale the efficacy of echogenicity in assessing plaque composition. In contrast to previous validation studies, this analysis included a large number of histological cross-sections obtained from human hearts and introduced a detailed

Table 3
Confusion matrix and classifier performance in region- and area-level analysis with 3 tissue types (ENC and LNC were combined in the NC class) based on ECHO and ECHO-NIRS classification in the test set.

		Histological classification			Validation metrics			
		F-PIT	NC	Calcific	Recall	Precision	F-score	Accuracy (%)
ECHO-classification	**Region-level analysis**							
	F-PIT	93	14	3	0.84	0.85	0.84	-
	NC	18	32	0	0.70	0.64	0.67	-
	Calcific	0	0	41	0.93	1.00	0.96	-
	Overall performance	-	-	-	0.83	0.83	0.83	82.6
	Area-level analysis							
	F-PIT (mm^2)	232.26	7.31	3.06	0.72	0.96	0.82	-
	NC (mm^2)	90.50	13.57	0.04	0.65	0.13	0.22	-
	Calcific (mm^2)	0.32	0.00	9.40	0.75	0.97	0.85	-
	Overall performance	-	-	-	0.72	0.91	0.79	71.6
ECHO-NIRS classification	**Region-level analysis**							
	F-PIT	111	20	3	1.00	0.83	0.91	-
	NC	0	26	0	0.57	1.00	0.72	-
	Calcific	0	0	41	0.93	1.00	0.96	-
	Overall performance	-	-	-	0.89	0.91	0.88	88.6
	Area-level analysis							
	F-PIT (mm^2)	318.99	10.59	3.09	0.99	0.96	0.97	-
	NC (mm^2)	3.77	10.29	0.01	0.49	0.73	0.59	-
	Calcific (mm^2)	0.32	0.00	9.40	0.75	0.97	0.85	-
	Overall performance	-	-	-	0.95	0.95	0.95	95.0

F-PIT, fibrotic or pathological intimal thickening; NC, necrotic core.

methodology for the identification of the different tissue types detected by histology on IVUS images. We found that the conventional echogenicity approach, which relies on discriminating tissue types on the basis of pixel intensity in relation to that of the adventitia, was very accurate in detecting calcific tissue but it often misclassified F-PIT as NC – a fact that at least partially should be attributed to the digital time gain compensation technique applied to improve image quality distal to the catheter probe in the NIRS-IVUS system, causing an increase in pixel brightness of the adventitia and thus an overestimation of the NC component (Fig. 2 and Supplementary Fig. 3).

To overcome this limitation and fully explore the potential of echogenicity we used the pixel intensity characteristics of different tissue types to train machine learning classifiers for more accurate assessment of plaque composition. This approach improved the overall performance of echogenicity but also underscored its indigenous limitations. The pixel intensities of F-PIT and ENC tissues were similar and thus this technique could not differentiate these two tissue types. Conversely, the mean pixel intensity of LNC was considerably lower than that of F-PIT and ENC, however the cut-offs identified by the J48 classifier did not allow accurate differentiation of F-PIT/ENC from LNC, as often F-PIT/ENC was misclassified as LNC and vice versa. The developed model did enable accurate detection of calcific tissue in region-level analysis while in area-level analysis we found that 23% of the calcific pixels were misclassified as F-PIT or F-PIT/ENC - this is likely due to the fact that calcific ROIs encompassed a wide pixel spectrum including some with lower intensity. Results however were improved in the test set where the calcific tissue had a more typical appearance. These findings are in line with histology studies showing that IVUS is capable of accurately detecting the presence of calcium but it has a limited efficacy in quantifying its area [36].

In contrast to echogenicity that has limited efficacy in identifying NC, NIRS has a high accuracy in detecting this tissue type. In the training set, 45 of the 49 LNCs and 20 of the 31 ENCs were located in yellow-spot regions. The incorporation of NIRS to tissue echogenicity markedly improved the efficacy of the model in detecting plaque composition. This is primarily due to hypoechogenic areas located outside the yellow-spots which were initially falsely classified by echogenicity as NC or LNC tissue being reclassified as F-PIT. This approach resulted in better recall for F-PIT detection, and precision for NC or LNC detection, but had no impact on recall for NC or LNC tissue which was mainly affected by the

Table 4
Confusion matrix and classifier performance in region and area-level analysis with 3 tissue types (F-PIT and ENC were combined in a single class) based on ECHO-classification and ECHO-NIRS classification in the test set.

		Histological classification			Validation metrics			
		F-PIT/ENC	LNC	Calcific	Recall	Precision	F-score	Accuracy (%)
ECHO-classification	**Region-level analysis**							
	F-PIT/ENC	116	6	3	0.84	0.93	0.88	-
	LNC	22	13	0	0.68	0.37	0.48	-
	Calcific	0	0	41	0.93	1.00	0.96	-
	Overall performance	-	-	-	0.85	0.89	0.86	84.6
	Area-level analysis							
	F-PIT/ENC (mm^2)	249.45	4.60	3.13	0.75	0.97	0.85	-
	LNC (mm^2)	80.70	8.86	0.04	0.66	0.10	0.17	-
	Calcific (mm^2)	0.32	0.00	9.34	0.75	0.97	0.84	-
	Overall performance	-	-	-	0.75	0.94	0.82	75.1
ECHO-NIRS classification	**Region-level analysis**							
	F-PIT/ENC	130	6	3	0.94	0.94	0.94	-
	LNC	8	13	0	0.68	0.62	0.65	-
	Calcific	0	0	41	0.93	1.00	0.96	-
	Overall performance	-	-	-	0.92	0.92	0.92	91.5
	Area-level analysis							
	F-PIT/ENC (mm^2)	324.31	6.78	3.16	0.98	0.97	0.98	-
	LNC (mm^2)	5.84	6.68	0.01	0.50	0.53	0.51	-
	Calcific (mm^2)	0.32	0.00	9.34	0.75	0.97	0.84	-
	Overall performance	-	-	-	0.95	0.95	0.95	95.5

ENC, early necrotic core; F-PIT, fibrotic or pathological intimal thickening; LNC, late necrotic core.

limited efficacy of echogenicity in differentiating F-PIT from ENC or LNC (Fig. 2 and Supplementary Fig. 3).

Results were similar in the test set - the ECHO-NIRS classifier had a marginally higher efficacy in detecting NC in region-level analysis and similar performance to the training set in area-level analysis. However, the model trained for LNC detection had lower performance for detecting this tissue type. This should be attributed to the fact that NIRS identified only 84% of the LNCs in the test set, compared to 92% in the training set, and to the fact that the ECHO classifier was less effective in detecting LNCs in this set compared to the training set. This had an impact on the overall accuracy of the ECHO classifier in the test set; however, the ECHO-NIRS approach had a similar overall classification performance to the training set for F-PIT/ENC, LNC and calcific tissue types. This finding highlights the robustness of the developed methodology in characterizing plaque composition and renders the combined ECHO-NIRS approach as one of the best methodologies reported in the literature for automated plaque characterization in intravascular images.

Radiofrequency analysis methods of the reflected IVUS signal have been used in the past to assess plaque composition and reports have shown that these can provide useful prognostic information [7,12,37–41]; however, recent studies have raised concerns about their reliability in delineating tissue components leading to their removal from clinical practice [35,42]. At present, only the integrated backscatter-IVUS analysis system is clinically available for plaque characterization in IVUS images, and this is only available in Japan.

In OCT, studies have shown promise in differentiating plaque components in superficial plaque [15,43–46]. However, OCT has poor signal penetration depth and this engenders difficulty in classification of deeper plaque components and the delineation of the external elastic membrane [47]. Moreover, the above methodologies have not been incorporated in user-friendly software. The only contemporary, commercially available tool for OCT plaque composition analysis includes a machine learning algorithm trained against the estimations of experts but not histology, approximating the external elastic membrane border in diseased segments, raising a concern about the accuracy of this approach in advanced atherosclerotic plaques [48].

Our approach overcomes these limitations as it was trained using histological estimations, has been validated in a discrete, independent test set, and has been incorporated in a user-friendly, commercially-available software – which also includes machine learning algorithms for fast and accurate segmentation of the IVUS images enabling analysis

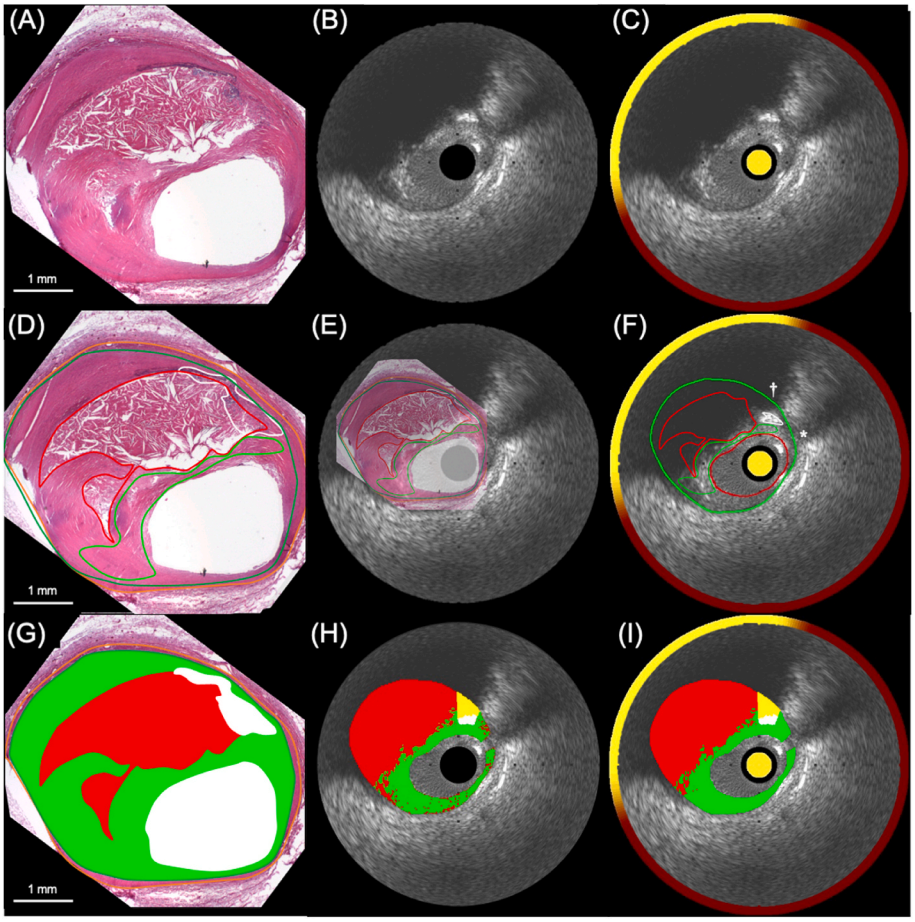

Fig. 2. Case example showing the methodology used to define the ROIs in a fibroatheroma in NIRS-IVUS images.
(A) The histological cross-section and (B and C) the corresponding IVUS and NIRS-IVUS frames. A histopathologist annotated the tissue types on the histological cross-section (D) that was then superimposed in the corresponding NIRS-IVUS image (E). This approach allowed determination of the location of the different tissue types on the NIRS-IVUS frame (F); the pixel intensities of the annotated ROIs were used to train a J48 classifier for detecting plaque composition (pixels corresponding to the guidewire artifact (indicated with a *) or to acoustic shadowing behind calcific tissue (indicated with a †) were excluded). (G) Tissue distribution in the histological cross-section. (H) The estimations of ECHO-classification, and (I) the estimations of ECHO-NIRS-classification – after classifying all the non-calcific pixels outside the yellow-spot area as F-PIT – for plaque composition. (For interpretation of the references to colour in this figure legend, the reader is referred to the Web version of this article.)

of large datasets and quantification of plaque components in a reproducible manner [49,50]. These advances are anticipated to promote the broad use of the combined ECHO-NIRS approach for plaque characterization in serial NIRS-IVUS studies evaluating the efficacy of novel pharmacotherapies on plaque evolution. Moreover, the developed methodology can be potentially incorporated in future NIRS-IVUS systems that will allow its use in the catheterization laboratory to facilitate PCI planning, while simultaneously allowing more accurate detection of high-risk lesions and patients enabling a personalized therapy of vulnerable individuals with novel systemic or focal therapies targeting atherosclerosis [51].

4.1. Limitations

There are several limitations in this report which must be acknowledged. One is that the number of histological cross-sections included in the analysis is small. This resulted in a relatively small number of ENC ROIs for training which may have not allowed the classifier to identify an optimal cut-off capable of differentiating ENC from F-PIT. Furthermore, we have excluded 24.3% of the data from the analysis because of the presence of artefacts or the inability to match histological slices with NIRS-IVUS images – this may have introduced bias. However, the consistency of the findings of our analysis in the training and test sets gives us confidence about the reproducibility of the reported results. Moreover, despite the fact that the ECHO-NIRS methodology is one of the best and well-validated methods in the literature, and is very accurate for detecting F-PIT and calcific tissue, its performance is only moderate for NC and LNC tissue detection – which have been associated with plaque disruption and cardiovascular events [52]. This should be attributed to the fact that both NIRS and especially echogenicity have limitations in identifying the presence and assessing the extent of lipid tissue. Considering however, that there is no widely-available method capable of accurately identifying plaque composition and also the fact that the ECHO-NIRS approach is fast and operates in user-friendly software we believe that this study is important in the field and that the proposed methodology will have broad clinical and research applications. In addition, although the matching between histology and IVUS cross-sections was performed by two expert analysts, errors in the co-registration of the IVUS and histological images are likely, as well as in the superimposition of the annotated tissues in the IVUS frames, which may have impacted the reported results. To minimize errors in these steps, two experts in intravascular imaging and a histopathologist conducted this part of the study and the final decisions about the co-registration of IVUS and histological images and about the location of the ROIs in IVUS frames were reached by consensus. Finally, in this study we assessed the efficacy of echogenicity in a 40 MHz IVUS system; further training is likely required in order for this approach to be applicable to wider bandwidth state-of-the-art catheters.

4.2. Conclusions

Echogenicity combined with the NIRS-signal information appears capable of accurately characterizing plaque composition in NIRS-IVUS images. This approach has been validated in an independent test set and incorporated in a user-friendly software enabling its broader use in research. Future studies are expected to allow us to examine the value of this approach in assessing the performance of novel therapies on plaque morphology and its potential advantage over standalone IVUS or NIRS in detecting vulnerable plaques and patients.

CRediT authorship contribution statement

Retesh Bajaj: Methodology, Investigation, Data curation, Formal analysis, Writing – original draft, Validation. **Jeroen Eggermont:** Methodology, Software, Validation, Writing – review & editing, and. **Stephanie J. Grainger:** Resources, Data curation, Writing – review & editing. **Lorenz Räber:** Writing – review & editing. **Ramya Parasa:** Writing – review & editing. **Ameer Hamid A. Khan:** Writing – review & editing. **Christos Costa:** Writing – review & editing. **Emrah Erdogan:** Writing – review & editing. **Michael J. Hendricks:** Resources, Data curation, Writing – review & editing, and. **Karthik H. Chandrasekharan:** Validation, Writing – review & editing. **Mervyn Andiapen:** Writing – review & editing. **Patrick W. Serruys:** Writing – review & editing. **Ryo Torii:** Writing – review & editing. **Anthony Mathur:** Writing – review & editing. **Andreas Baumbach:** Writing – review & editing. **Jouke Dijkstra:** Methodology, Software, Validation, Writing – review & editing. **Christos V. Bourantas:** Methodology, Formal analysis, Project administration, Writing – review & editing, Supervision.

Declaration of competing interests

The authors declare the following financial interests/personal relationships which may be considered as potential competing interests: MJH and SJG are employees of Infraredx. All other authors have no conflicts of interests to declare.

Acknowledgements

The authors wish to acknowledge the Cardiovascular Devices Hub at the Centre for Cardiovascular Medicine and Devices, Queen Mary University of London for supporting the present study. RB, RP, MA, AM, AB and CVB are funded by Barts NIHR Biomedical Research Centre, London, UK.

Appendix A. Supplementary data

Supplementary data to this article can be found online at https://doi.org/10.1016/j.atherosclerosis.2022.01.021.

References

[1] R. Hoffmann, G.S. Mintz, J.J. Popma, et al., Treatment of calcified coronary lesions with Palmaz-Schatz stents. An intravascular ultrasound study, Eur. Heart J. 19 (1998) 1224–1231.
[2] C.V. Bourantas, Y.-J. Zhang, S. Garg, et al., Prognostic implications of coronary calcification in patients with obstructive coronary artery disease treated by percutaneous coronary intervention: a patient-level pooled analysis of 7 contemporary stent trials, Heart 100 (2014) 1158–1164.
[3] T. Lee, T. Kakuta, T. Yonetsu, et al., Assessment of echo-attenuated plaque by optical coherence tomography and its impact on post-procedural creatine kinase-myocardial band elevation in elective stent implantation, JACC Cardiovasc. Interv. 4 (2011) 483–491.
[4] Y.J. Hong, M.H. Jeong, Y.H. Choi, et al., Impact of plaque components on no-reflow phenomenon after stent deployment in patients with acute coronary syndrome: a virtual histology-intravascular ultrasound analysis, Eur. Heart J. 32 (2011) 2059–2066.
[5] A. Tanaka, T. Imanishi, H. Kitabata, et al., Lipid-rich plaque and myocardial perfusion after successful stenting in patients with non-ST-segment elevation acute coronary syndrome: an optical coherence tomography study, Eur. Heart J. 30 (2009) 1348–1355.
[6] F. Prati, oboC. Investigators, E. Romagnoli, et al., Relationship between coronary plaque morphology of the left anterior descending artery and 12 months clinical outcome: the CLIMA study, Eur. Heart J. 41 (2020) 383–391.
[7] G.W. Stone, A. Maehara, A.J. Lansky, et al., A prospective natural-history study of coronary atherosclerosis, N. Engl. J. Med. 364 (2011) 226–235.
[8] R. Waksman, C.D. Mario, R. Torguson, et al., Identification of patients and plaques vulnerable to future coronary events with near-infrared spectroscopy intravascular ultrasound imaging: a prospective, cohort study, Lancet 394 (2019) 1629–1637.
[9] D. Erlinge, A. Maehara, O. Ben-Yehuda, et al., Identification of vulnerable plaques and patients by intracoronary near-infrared spectroscopy and ultrasound (PROSPECT II): a prospective natural history study, Lancet 397 (2021) 985–995.
[10] N. Bruining, S. Verheye, M. Knaapen, et al., Three-dimensional and quantitative analysis of atherosclerotic plaque composition by automated differential echogenicity, Cathet. Cardiovasc. Interv. 70 (2007) 968–978.
[11] A. Nair, B.D. Kuban, E.M. Tuzcu, et al., Coronary plaque classification with intravascular ultrasound radiofrequency data analysis, Circulation 106 (2002) 2200–2206.
[12] A. Nair, M.P. Margolis, B.D. Kuban, et al., Automated coronary plaque characterisation with intravascular ultrasound backscatter: ex vivo validation, EuroIntervention, J. EuroPCR Collaboration Work. Group Interventional Cardiol. Eur. Soc. Cardiol. 3 (2007) 113–120.
[13] M. Kawasaki, H. Takatsu, T. Noda, et al., In vivo quantitative tissue characterization of human coronary arterial plaques by use of integrated backscatter intravascular ultrasound and comparison with angioscopic findings, Circulation 105 (2002) 2487–2492.
[14] J.C. Teo, N. Foin, F. Otsuka, et al., Optimization of coronary optical coherence tomography imaging using the attenuation-compensated technique: a validation study, Eur. Heart J. Cardiovasc. Imag. 18 (2017) 880–887.
[15] C. Xu, J.M. Schmitt, S.G. Carlier, et al., Characterization of atherosclerosis plaques by measuring both backscattering and attenuation coefficients in optical coherence tomography, J. Biomed. Opt. 13 (2008), 034003.
[16] S. Liu, Tissue characterization with depth-resolved attenuation coefficient and backscatter term in intravascular optical coherence tomography images, J. Biomed. Opt. 22 (2017) 1.
[17] C. He, Z. Li, J. Wang, et al., Atherosclerotic plaque tissue characterization: an OCT-based machine learning algorithm with ex vivo validation, Front. Bioeng. Biotechnol. 8 (2020).
[18] J. Lee, D. Prabhu, C. Kolluru, et al., Automated Plaque Characterization Using Deep Learning on Coronary Intravascular Optical Coherence Tomographic Images, vol. 10, Biomedical Optics Express, 2019.
[19] S.-J. Kang, G.S. Mintz, J. Pu, et al., Combined IVUS and NIRS detection of fibroatheromas, JACC (J. Am. Coll. Cardiol.): Cardiovasc. Imag. 8 (2015) 184–194.
[20] C.M. Gardner, H. Tan, E.L. Hull, et al., Detection of lipid core coronary plaques in autopsy specimens with a novel catheter-based near-infrared spectroscopy system, JACC Cardiovasc. Imag. 1 (2008) 638–648.
[21] F. Otsuka, M.C.A. Kramer, P. Woudstra, et al., Natural progression of atherosclerosis from pathologic intimal thickening to late fibroatheroma in human coronary arteries: a pathology study, Atherosclerosis 241 (2015) 772–782.
[22] R. Virmani, F.D. Kolodgie, A.P. Burke, et al., Lessons from sudden coronary death: a comprehensive morphological classification scheme for atherosclerotic lesions, Arterioscler. Thromb. Vasc. Biol. 20 (2000) 1262–1275.
[23] G.S. Mintz, S.E. Nissen, R.A. O'Rourke, American college of cardiology clinical expert consensus document on standards for acquisition, measurement and reporting of intravascular ultrasound studies (IVUS). A report of the American college of cardiology task force on clinical expert consensus documents, J. Am. Coll. Cardiol. 37 (2001) 15.
[24] S.A. de Winter, I. Heller, R. Hamers, et al., Computer assisted three-dimensional plaque characterization in intracoronary ultrasound studies, Comput. Cardiol. 2003 (2003) 73–76.
[25] M. H, M.N. S, A review on evaluation metrics for data classification evaluations, Int. J. Data Min. Knowl. Process Manag. 5 (2015), 01-11.
[26] J. Lever, M. Krzywinski, N. Altman, Classification evaluation, Nat. Methods 13 (2016) 603–604.
[27] E.J. Gussenhoven, C.E. Essed, C.T. Lancée, et al., Arterial wall characteristics determined by intravascular ultrasound imaging: an in vitro study, J. Am. Coll. Cardiol. 14 (1989) 947–952.
[28] F. Prati, Correlation between high frequency intravascular ultrasound and histomorphology in human coronary arteries, Heart 85 (2001) 567–570.
[29] B.N. Potkin, A.L. Bartorelli, J.M. Gessert, et al., Coronary artery imaging with intravascular high-frequency ultrasound, Circulation 81 (1990) 1575–1585.
[30] X. Wu, G.S. Mintz, K. Xu, et al., The relationship between attenuated plaque identified by intravascular ultrasound and No-reflow after stenting in acute myocardial infarction, JACC Cardiovasc. Interv. 4 (2011) 495–502.
[31] S.Y. Lee, G.S. Mintz, S.-Y. Kim, et al., Attenuated plaque detected by intravascular ultrasound, JACC Cardiovasc. Interv. 2 (2009) 65–72.
[32] Y. Shiono, T. Kubo, A. Tanaka, et al., Impact of attenuated plaque as detected by intravascular ultrasound on the occurrence of microvascular obstruction after percutaneous coronary intervention in patients with ST-segment elevation myocardial infarction, JACC, Cardiovasc. Interv. 6 (2013) 847–853.
[33] D. Shishikura, Y. Kataoka, G. Di Giovanni, et al., Progression of Ultrasound Plaque Attenuation and Low Echogenicity Associates with Major Adverse Cardiovascular Events, European Heart Journal, 2020 ehaa173.
[34] J. Pu, G.S. Mintz, S. Biro, et al., Insights into echo-attenuated plaques, echolucent plaques, and plaques with spotty calcification, J. Am. Coll. Cardiol. 63 (2014) 2220–2233.
[35] J.F. Granada, D. Wallace-Bradley, H.K. Win, et al., In vivo plaque characterization using intravascular ultrasound–virtual histology in a porcine model of complex coronary lesions, Arterioscler. Thromb. Vasc. Biol. 27 (2007) 387–393.
[36] T. Kume, H. Okura, T. Kawamoto, et al., Assessment of the coronary calcification by optical coherence tomography, EuroIntervention, J. EuroPCR Collaboration Work. Group Interventional Cardiol. Eur. Soc. Cardiol. 6 (2011) 768–772.
[37] C.M. Campos, R.J. Fedewa, H.M. Garcia-Garcia, et al., Ex vivo validation of 45 MHz intravascular ultrasound backscatter tissue characterization, Eur. Heart J. Cardiovasc. Imag. 16 (2015) 1112–1119.
[38] P.A. Calvert, D.R. Obaid, M. O'Sullivan, et al., Association between IVUS findings and adverse outcomes in patients with coronary artery disease: the VIVA (VH-IVUS

in vulnerable atherosclerosis) study, JACC (J. Am. Coll. Cardiol.): Cardiovasc. Imag. 4 (2011) 894–901.
[39] J.M. Cheng, H.M. Garcia-Garcia, S.P.M. de Boer, et al., In vivo detection of high-risk coronary plaques by radiofrequency intravascular ultrasound and cardiovascular outcome: results of the ATHEROREMO-IVUS study, Eur. Heart J. 35 (2014) 639–647.
[40] M. Okubo, M. Kawasaki, Y. Ishihara, et al., Development of integrated backscatter intravascular ultrasound for tissue characterization of coronary plaques, Ultrasound Med. Biol. 34 (2008) 655–663.
[41] S. Sathyanarayana, S. Carlier, W. Li, et al., Characterisation of atherosclerotic plaque by spectral similarity of radiofrequency intravascular ultrasound signals, EuroIntervention: J. EuroPCR Collaboration Work. Group Interventional Cardiol. Eur. Soc. Cardiol. 5 (2009) 133–139.
[42] T. Thim, M.K. Hagensen, D. Wallace-Bradley, et al., Unreliable assessment of necrotic core by virtual histology intravascular ultrasound in porcine coronary artery disease, Circulation: Cardiovasc. Imag. 3 (2010) 384–391.
[43] G. van Soest, T. Goderie, E. Regar, et al., Atherosclerotic tissue characterization in vivo by optical coherence tomography attenuation imaging, J. Biomed. Opt. 15 (2010).
[44] L.S. Athanasiou, C.V. Bourantas, G. Rigas, et al., Methodology for fully automated segmentation and plaque characterization in intracoronary optical coherence tomography images, J. Biomed. Opt. 19 (2014).
[45] J.C. Teo, N. Foin, F. Otsuka, et al., Optimization of coronary optical coherence tomography imaging using the attenuation-compensated technique: a validation study, Eur. Heart J. Cardiovasc. Imag. (2016) jew153.
[46] S. Liu, Tissue characterization with depth-resolved attenuation coefficient and backscatter term in intravascular optical coherence tomography images, J. Biomed. Opt. 22 (2017).
[47] O. Manfrini, E. Mont, O. Leone, et al., Sources of error and interpretation of plaque morphology by optical coherence tomography, Am. J. Cardiol. 98 (2006) 156–159.
[48] M. Chu, H. Jia, J.L. Gutierrez-Chico, et al., Automatic Characterisation of Human Atherosclerotic Plaque Composition from Intravascular Optical Coherence Tomography Using Artificial Intelligence, EuroIntervention, 2021.
[49] R. Bajaj, X. Huang, Y. Kilic, et al., Advanced deep learning methodology for accurate, real-time segmentation of high-resolution intravascular ultrasound images, Int. J. Cardiol. 339 (2021) 185–191. https://www.internationaljournalofcardiology.com/article/S0167-5273(21)01028-7/fulltext#%20.
[50] E. Erdogan, X. Huang, J. Cooper, et al., End-diastolic Segmentation of Intravascular Ultrasound Images Enables More Reproducible Volumetric Analysis of Atheroma Burden, Catheterization and Cardiovascular Interventions, 2021.
[51] C.V. Bourantas, H.M. Garcia-Garcia, R. Torii, et al., Vulnerable plaque detection: an unrealistic quest or a feasible objective with a clinical value? Heart 102 (2016) 581–589.
[52] C.V. Felton, D. Crook, M.J. Davies, et al., Relation of plaque lipid composition and morphology to the stability of human aortic plaques, Arterioscler. Thromb. Vasc. Biol. 17 (1997) 1337–1345.